Astron. Astrophys. 82, 30–40 (1980)

ASTRONOMY AND ASTROPHYSICS

A Model for Sunspot Associated Emission at 6 cm Wavelength

C. E. Alissandrakis[1]*, M. R. Kundu[2], and P. Lantos[3]

[1] Department of Astronomy, University of Athens Panepistimiopolis, Athens 621, Greece
[2] Astronomy Program, University of Maryland, College Park, Maryland 20742, USA
[3] Observatoire de Paris, F-92190 Meudon, France

Received February, 22, 1979

Summary. We have calculated 2-dimensional maps of total intensity and circular polarization of a sunspot region at 6 cm using a simple model for the chromosphere-corona transition region and observations of the longitudinal component of the photospheric magnetic field. The calculations are in good agreement with the high resolution observations of the same sunspot region at 6 cm, obtained with the Westerbork Synthesis Radio Telescope. We show that the 6 cm radiation is predominatly due to gyroresonance absorption process at the second and third harmonics of the gyrofrequency ($H=900$–600 G). Estimates of the conductive flux and the electron density in the transition region above the sunspot are also given.

Key words: radio emission – sunspots – transition region

I. Introduction

High resolution observations at centimeter wavelengths (Kundu, 1959; Kundu and Alissandrakis, 1975; Alissandrakis, 1977; Kundu et al., 1977, hereafter referred to as Paper I; Felli et al., 1977) of solar active regions consisting of sunspots and plages have shown that the very intense emission is usually associated with sunspots, while the weaker emission is associated with chromospheric plages or with regions of transverse magnetic field.

The sunspot associated component has been interpreted as arising mainly from emission at the harmonics of the gyrofrequency (Zheleznyakov, 1962; Kakinuma and Swarup, 1962). Zlotnik (1968a, b) calculated the spectrum of a model sunspot and showed that it was in good agreement with the observations. One-dimensional intensity scans across a bipolar sunspot group calculated by Lantos (1968) at 6 cm showed significant structure and center to limb variation. These calculations were performed by using idealized models of the magnetic field and were compared with the observations of "average" active regions. The observational basis of these models was the form of the intensity and polarization spectrum and the core-halo structure of the active regions at cm-λ. It is clear that high resolution observations of the cm-λ emission with simultaneous measurements of the photospheric magnetic field will permit a better study of the processes involved, as well as of the physical conditions above active regions. The observations reported by Kundu et al. (1977) have provided the opportunity for such a study.

Send offprint requests to: M. R. Kundu
* Present address: Department of Astrophysics, University of Athens, Greece

In the present paper we present calculations of the 6 cm radio emission from a region above a sunspot, using the observed photospheric magnetic field and simple models of electron temperature and density. The results are compared with the high resolution observations of the same region, described in Paper I. We have confirmed that gyroresonance is the dominant emission mechanism at this wavelength, and as a consequence we have obtained information about the magnetic field, temperature and density of the transition region above the sunspot.

We should note here that so far only the radio observations are capable of providing a direct measurement of the magnetic field above the photospheric level. As for the temperature and density structure in the transition region, information has been obtained from EUV observations (Foukal et al., 1974; Foukal, 1975 and 1976) and it will be interesting to compare the cm-λ and the EUV results. In the following sections we briefly describe our observations (see Paper I for details); we then discuss our model calculations and compare them with the observations.

II. Observations

Our 6 cm observations were obtained in 1974, May 8–10 with the Westerbork Synthesis Radio Telescope which provided a resolution of 6″ in the E-W direction and 22″ in the N-S direction (Paper I). The instrument provides 12 h synthesis maps of all four Stokes parameters I, Q, U, and V.

Of the four active regions that were observed, we selected for model calculations the western part of McMath region 12906 (Region 3 in Paper I) observed on May 9. The maps of this region in total intensity I and circular polarization V are shown in Fig. 1; no linear polarization was detected. The region was located at S07 W37 on May 9. After correction for the instrumental resolution the brightness temperature of the sunspot associated component came to $1.25\ 10^6$ K. This region had the advantage that it contained only one big sunspot and a smaller one; therefore we expected a fairly simple magnetic field structure. In addition, it showed some interesting features, namely a sharp drop of intensity in the direction towards the limb and a double peaked circular polarization structure.

The observations of the longitudinal component of the photospheric magnetic field were obtained by Rayrole with the Meudon Magnetograph on May 9, using the λ 5225 Fe I line. The instrument and the observing procedure have been described by Rayrole (1967); a photograph of the Zeeman pattern is obtained and subsequently the displacement of the line is measured with the "lamb-

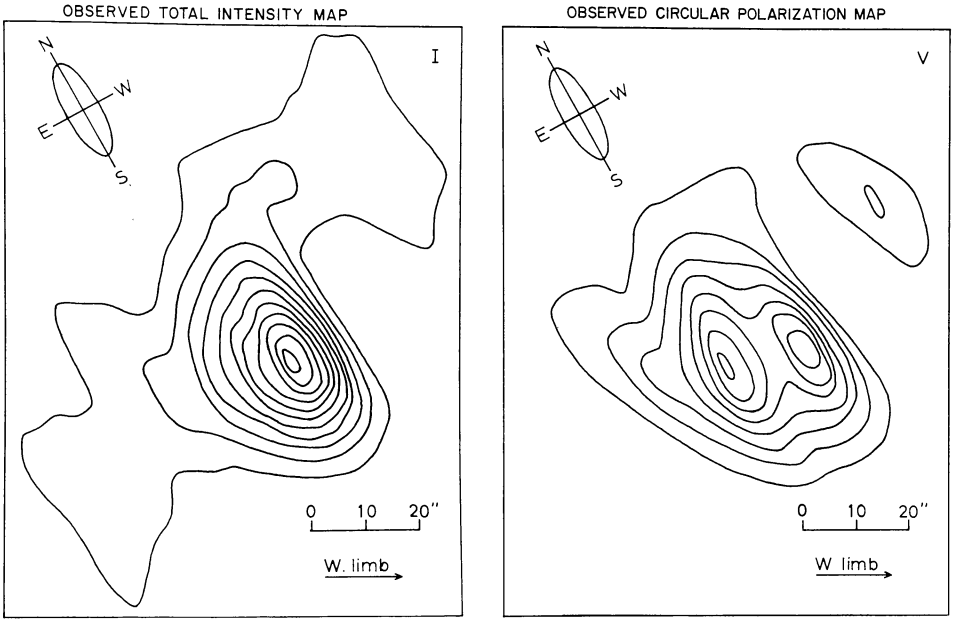

Fig. 1a. Total intensity (I) and b circular polarization (V) maps at 6 cm of the west part of McMath region 12906 on May 9, 1974, obtained with the Westerbork Synthesis Radio Telescope. The contour levels are 7.5 10^4–8.25 10^5 K in steps of 7.5 10^4 K for the I map and 2.25 10^4–1.8 10^5 K in steps of 2.25 10^4 K for the V map

dameter". The measurement of the displacement, rather than the intensity difference at two fixed wavelengths of the line, avoids saturation at high sunspot magnetic fields.

III. Emission Mechanisms

In a magnetoionic medium, such as the solar atmosphere, the electromagnetic radiation can, in general, be described in terms of two waves, the ordinary and the extraordinary. The brightness temperature, T_b, of each mode is given by the well known solution of the transfer equation;

$$T_{b,j}=\int_0^\infty T(\tau_j)\exp(-\tau_j)d\tau_j \tag{1}$$

where $T(\tau_j)$ is the electron temperature at optical depth, τ_j, and the integration is carried along the path of the radiation, which may be curved if the refraction index is not unity. We shall use the designation $j=1$ for the extraordinary mode and $j=2$ for the ordinary mode. The optical depth is given by:

$$d\tau_j=-\mu_j ds \tag{2}$$

where μ_j is the absorption coefficient and ds is an infinitesimal path length. The absorption coefficient consists of two contributory components due to (1) free-free (or Bremsstrahlung, here referred to as $f-f$) and (2) gyroresonance ($g-r$) processes:

$$\mu_j=\mu_j^{f-f}+\mu_j^{g-r}. \tag{3}$$

Free-free radiation is emitted by thermal electrons in the presence of the electric field of the ions. The $f-f$ absorption coefficient is of the form (Kundu, 1965):

$$\mu_j^{f-f}=\frac{\zeta}{f^2}\frac{N^2}{T^{3/2}}B_j(H,\theta) \tag{4}$$

where N is the electron density and for low densities B_j is a function of only the magnitude of the magnetic field, H and the angle between the direction of the field and the radiation path, θ; ζ is a slowly varying function of N and T, and f is the observing frequency. For non-zero magnetic field the opacity of the extraordinary mode increases while that of the ordinary mode decreases, compared to their values at zero magnetic field; both modes have a slow variation of opacity with θ.

In the presence of a magnetic field the thermal electrons emit $g-r$ radiation as they spiral around the lines of force. The $g-r$ absorption has sharp peaks at frequencies f such that f is a harmonic of the local electron gyrofrequency, f_H, (i.e. when $f=lf_H$, l an integer). At $\lambda=6$ cm, resonance absorption occurs for values of the magnetic field, $H=1790$ G ($l=1$), 895 G ($l=2$), 597 G ($l=3$). The absorption coefficient is given by (Zheleznyakov, 1970):

$$\mu_j^{g-r}=\frac{l^{2l}}{2^l l}\frac{NT^{l-3/2}}{f}C_j(H,\theta)\exp\left[-\frac{1}{2}\left(\frac{x/L_H}{\beta\cos\theta}\right)^2\right] \tag{5}$$

where C_j is a function of H and θ only for low densities and has a very sharp variation with θ; x is the distance from the resonance level of a point at which $g-r$ absorption is considered, $\beta=1.299\ 10^{-5}\ T^{1/2}$ and $L_H=\left(\frac{1}{H}\frac{dH}{dx}\right)^{-1}$ is the scale length of the magnetic field. The absorption drops fast as the value of the local gyrofrequency departs from f/l; the full width at half maximum of a resonant layer at constant temperature is:

$$W=(\ln 256)^{1/2}L_H\beta\cos\theta \tag{6}$$

which is about 400 km for $\theta=0$, $T=2\ 10^6$ K and $L_H=10^9$ cm.

a) Relative Importance of Free-free and Gyroresonance Absorption Processes

Before we give numerical results it may be instructive to discuss the contributions to the radio emission above sunspots from the free-free and gyroradiation processes. Arguments in favor of the $g-r$ process have been given by Zheleznyakov (1962) and Kakinuma and Swarup (1962), based on the study of the intensity and polarization spectrum, as well as the brightness temperature and core-halo source structure (Kundu, 1959). Although we have no spectral information we have much more precise information on source structure in both total intensity and polarization, and

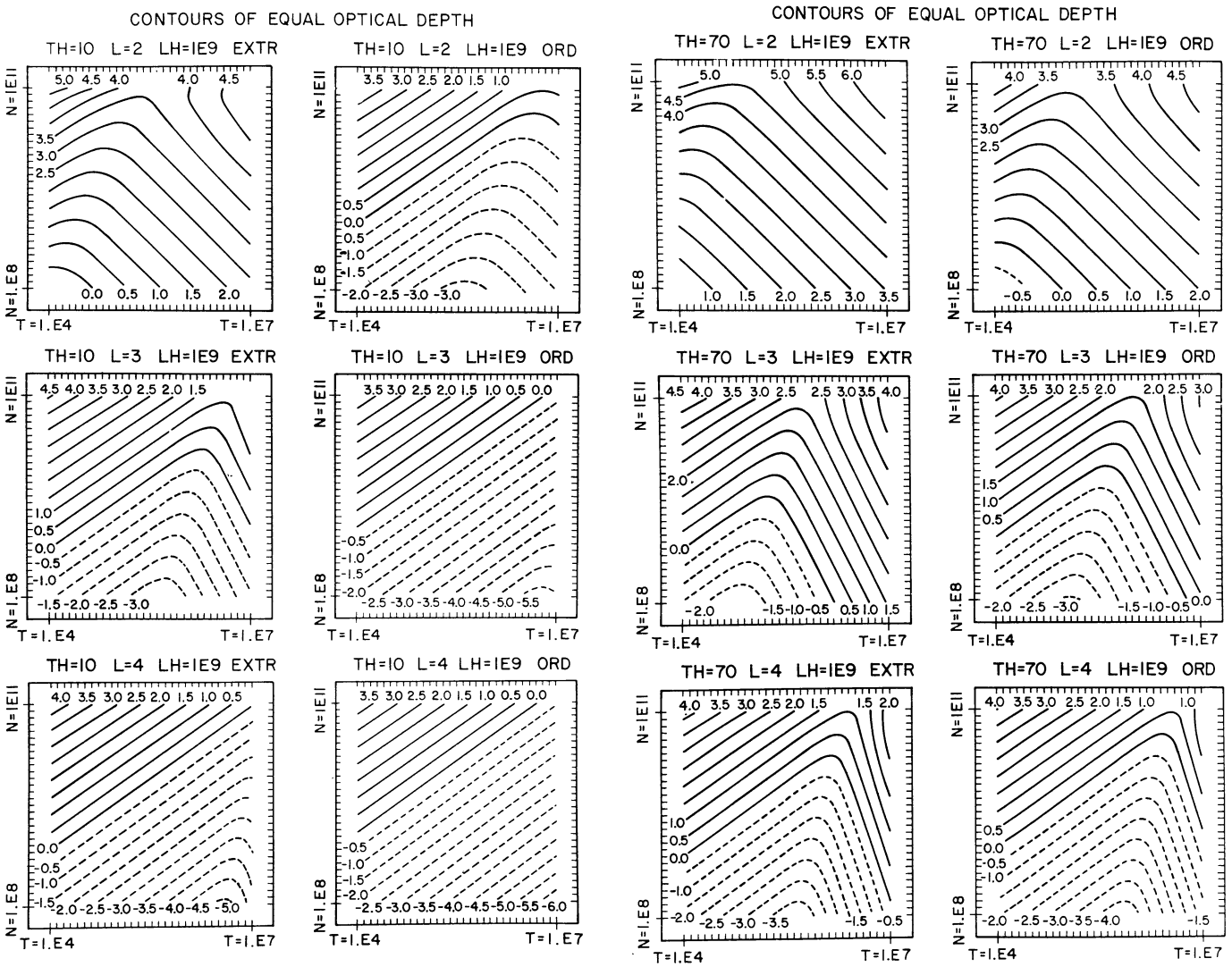

Fig. 2a and b. Contour maps of the total optical depth (f–f and g–r) of layers centered at resonant levels, as a function of electron density and temperature. The labels are the logarithm of the optical depth, dashed contours indicate $\tau<1$; L is the harmonic number, TH the angle between the direction of the magnetic field and the line of sight. a $TH=10°$ **b** $TH=70°$

brightness temperature. Our discussion will be based on these new results obtained with 6″ arc resolution.

The absorption coefficient of the $f-f$ process is considerably less than that of $g-r$ if the angle θ between the direction of the magnetic field and the line of sight is not close to zero; this by itself does not imply that $g-r$ is more important, because the vertical extent of the $f-f$ emitting region is much larger than the width of the resonance absorption layer. From Eqs. (2), (4) and (5) it is easy to see that for small densities $\tau^{g-r}\sim NT^{l-1}$ and $\tau^{f-f}\sim N^2T^{-3/2}$; thus the ratio of the $g-r$ to $f-f$ optical depths, under the same physical conditions, is proportional to $T^{l+1/2}N^{-1}$. Consequently $g-r$ is favored by high temperatures and low densities (i.e. coronal conditions) while $f-f$ emission is favored by low temperatures and high densities (i.e. chromospheric conditions).

In order to discuss more quantitatively the relative contributions of the two processes, we have calculated the total optical depth at 6 cm of a layer centered at the l^{th} harmonic and extending from the point where $f=(l+1/2)f_H$ to the point where $f=(l-1/2)f_H$. We have assumed constant N, T, and θ and a linear decrease of the magnetic field with height with $L_H=10^9$ cm. The results are shown in Fig. 2 in the form of contour plots of the logarithm of the total optical depth as a function of electron temperature and density. Dashed contour lines correspond to $\tau<1$. The calculations were performed for both ordinary and extraordinary modes at the second, third and fourth harmonic for $\theta=10°$ (Fig. 2a) and $\theta=70°$ (Fig. 2b).

There are two regions in each plot: in the $T-N$ range where $f-f$ dominates the slope of the contour lines is positive (i.e. for constant τ the density must increase to compensate for a temperature increase); in the range where $g-r$ dominates the slope of the contour lines is negative (i.e. the density must decrease as the temperature increases in order to keep τ constant). In some cases $f-f$ dominates for most of the temperatures and densities considered here (e.g. the fourth harmonic, ordinary mode, $\theta=10°$), while in other cases $g-r$ dominates entirely (e.g. the second harmonic, extraordinary mode, $\theta=70°$).

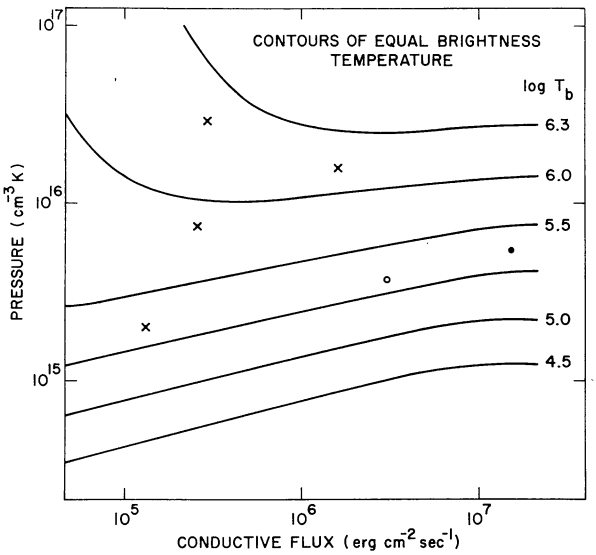

Fig. 3. Brightness temperature at 6 cm of the transition region and the corona as a function of conductive flux and the pressure at the base of the transition region. The corona is assumed isothermal at a temperature of $2.6\ 10^6$ K. The points show the values of pressure and conductive flux derived from EUV observations (open circle: Noyes et al. (1970); filled circle: Dupree et al. (1973); crosses: Jordan (1976)]

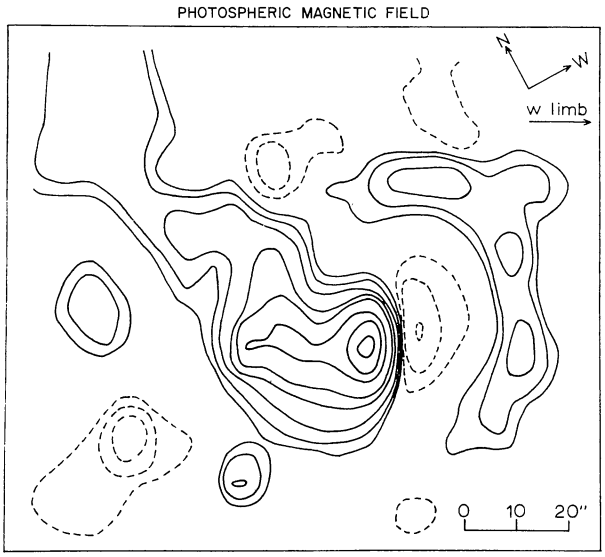

Fig. 4. Map of the longitudinal component of the photospheric Magnetic field on region 12906 on May 9 obtained with the Meudon magnetograph. The contour levels are ± 25, ± 50, ± 100, 200, 300, 500, 700, and 900 G; dashed contours indicate negative values

---

From Fig. 2, it is obvious that $g-r$ is dominant at high T, low harmonic numbers (i.e. high magnetic field) and large θ. Gyroresonance is not an effective opacity agent at the fourth harmonic, except at very high temperatures and large values of the angle θ; this implies that higher harmonics, which are optically thinner than the fourth, are also transparent. At the third harmonic $g-r$ is effective mainly at large angles, while the second harmonic is opaque, except at very small angles.

From observations at 2.8 cm with a 16″ fan beam, Felli et al. (1975), concluded that some compact sources could be interpreted as arising from $g-r$ emission at the fourth or fifth harmonic and large θ. In their arguments they considered only the ratio of the $g-r$ and $f-f$ optical depth and not the value of the optical depth itself; a calculation of τ for reasonable values of T_e and N_e for $\theta \approx 85°$ and $l=4$ gives $\tau_1 \approx 0.6$ while τ is less than 0.1 at the fourth harmonic for the ordinary mode and at the fifth harmonic for both modes. Thus even at 2.8 cm one has to resort to emission from the third or second harmonic.

We conclude that, for strong $g-r$ emission at 6 cm, the magnetic field must be such that the harmonics $l=2$ or $l=3$ ($H=900$ or 600 G) be located in the upper T.R. or the corona. This conclusion is still valid for $g-r$ even if the temperature is not constant, provided that it does not change too abruptly to make the height dependence of the $g-r$ absorption coefficient much different from a gaussian

b) Brightness Temperature of Free-free Emission

When the magnetic field above the chromosphere is below 600 G the $f-f$ process is the main opacity agent at 6 cm. We will now consider whether $f-f$ emission alone can account for the high brightness temperature of the sunspot-associated components as well as for the high contrast between sunspot and plage-associated components.

In previous papers (e. g. Felli et al., 1975; Chiuderi-Drago et al., 1977) the free-free emission has been treated as originating in a region of constant temperature. This is not a good assumption if the region of formation extends into the transition region (T. R.). Here we will treat separately the emission from the corona and the T. R. Considering the corona as isothermal at temperature T_{cor} and in hydrostatic equilibrium, the optical depth, τ_{cor} can be calculated from Eqs. (2) and (3):

$$\tau_{cor} = 0.5\ \mu_{cor} h \tag{7}$$

where μ_{cor} is the $f-f$ absorption coefficient at the base of the corona and h is the density scale height. This calculation assumes constant acceleration of gravity, which is not a bad assumption since only the low corona has any significant contribution. The coronal optical depth at 6 cm is less than 1 for coronal density less than about 10^{10} cm^{-3}.

The T. R. we write Eq. (2) in terms of the inverse temperature gradient dz/dT:

$$d\tau_j = \mu_j^{f-f} \frac{dz}{dT} dT. \tag{8}$$

The inverse temperature gradient can be expressed in terms of the conductive flux, F_c (cf. Athay, 1971)

$$\frac{dz}{dT} = \frac{A}{F_c} T^{5/2} \tag{9}$$

where $A = 1.1\ 10^{-6}$ cgs units. Taking the absorption coefficient from Eq. (4) we get

$$d\tau_j = \Gamma_j \frac{dT}{T} \tag{10}$$

where $\Gamma_j = \zeta p^2 A B_j / (f^2 F_c)$ and $p = NT$ is proportional to the electron pressure. Assuming constant conductive flux, constant pressure and constant magnetic field, Eq. (10) can be integrated over a

layer extending from $T=T_1$ to $T=T_2$ ($T_2>T_1$), to give

$$\tau_j=\Gamma_j \ln (T_2/T_1) \quad (11)$$

Subsequent integration of the transfer Eq. (1) gives

$$T_{b,j}=[T_2-T_1 \exp(-\tau_j)]\Gamma_j/(\Gamma_j+1). \quad (12)$$

According to some EUV models the conductive flux is taken to be constant in the T. R. for temperatures between 10^5 and 10^6 K. As a matter of fact, the relevant equations involve the term p^2/F_c, the pressure being assumed constant due to the narrow width of the T. R. Thus the assumption of constant Γ_j is not bad, considering also the fact that B_j is not a very sensitive function of the magnetic field.

We have calculated the brightness temperature of the corona and the T. R. above 10^5 K at the center of the disk assuming a magnetic field of 450 G (so that $g-r$ is not important) and for a range of possible values of p and F_c and for a coronal temperature of 2.6 10^6 K. For F_c less than about 10^6 erg cm^{-2} s^{-1} the T. R. becomes fairly extended and we have substituted the assumption of constant Γ_j with the assumptions of constant F_c and hydrostatic equilibrium; in this case the computation was done numerically and the value of the pressure refers to the base of the T. R. The results are presented in Fig. 3 which shows the relation between the values of p and F_c that give constant brightness temperature. In the same figure we have plotted the results on active regions of Noyes et al. (1970), Dupree et al. (1973), and Jordan (1976).

As expected from Eqs. (8)–(12) the brightness temperature is high for large values of p (i. e. high electron density) and low values of F_c (i. e. extended T. R.). In principle, brightness temperatures above 10^6 K could be produced in $p>10^{16}$ K cm^{-3} (Fig. 3); this is indeed the case in two of Jordan's (1976) models. However, from such an interpretation it follows that the density enhancement is limited only in the region directly above the sunspot; this would be necessary for the explanation of the sunspot-plage intensity difference which cannot be attributed to the effect of the magnetic field. There is no evidence of such a density enhancement in the Skylab observations of active regions in the EUV (Foukal et al., 1974; Foukal, 1976). These observations indicate that the pressure in the T. R. above sunspots may be less than the average of the active region.

The other possibility for significant contribution from the $f-f$ process is through a decrease in the conductive flux in the T. R., directly above the sunspots. The Skylab observations have shown such a decrease. However, a low conductive flux means a low temperature gradient; this, combined with the assumption of hydrostatic equilibrium implies that the density will be too low in regions of high temperature for significant $f-f$ emission. As it is shown in Fig. 3, even for very low values of the conductive flux the brightness temperature will not exceed 10^6 K unless $p>10^{16}$ K cm^{-3}.

We conclude that an extended T. R. cannot explain the sunspot associated 6 cm emission as originating predominantly from the $f-f$ process; consequently it is essential to have strong magnetic fields at high temperatures to make the $g-r$ process effective and consistent with the observations.

IV. Physical Conditions in the Transition Region Above Sunspots

From the above, it follows that for the computation of brightness temperatures, we must have a model of the temperature, density and magnetic field in the region of formation of the radiation. Our observations give the values of intensity and circular polarization at each point of the sunspot associated region. From these we can get the brightness temperatures of the ordinary and extraordinary wave modes. It is clear that from these two quantities alone we cannot construct detailed models of the radio emitting region; therefore we have employed very simple models of T, N, and H. A potential (current-free) model of the magnetic field has been used and we have assumed that the temperature and density vary only in the direction perpendicular to the solar surface.

Starting with a given model we have computed maps of the expected intensity and circular polarization, which were then convolved with the interferometer beam pattern. From a comparison of the computed and observed maps we have attempted to determine the parameters characterizing the best model. These parameters refer to some average physical conditions over the entire spot associated region; however, as we will discuss later, some parameters affect mainly the central part while others affect the edges of the region. We first discuss the models adopted.

a) Temperature and Density Models

The observed brightness temperature above sunspots is always of the order of 10^6 K. Since the brightness temperature of thermal radiation is equal to or less than the local electron temperature, the region of formation of the radiation must be in the transition region (T. R.) or in the corona. Therefore, in this paper, we have considered the transfer of radiation in the region of temperatures from 2 10^4 K up to coronal temperatures.

Models of the transition region, both in the active and quiet Sun have been obtained in the past decade from low-resolution EUV observations (Dupree and Goldberg, 1967; Withbroe, 1970; Noyes et al., 1970; Athay, 1971). The temperature structure of these models is determined by a constant conductive flux in the region of $T=10^5$–10^6 K and either constant pressure or hydrostatic equilibrium is assumed. With the availability of high resolution EUV observations, some authors have studied the physical conditions above spots. The observations indicate that low temperature regions exist at the center of sunspots up to considerable heights above the photosphere (Foukal, 1975; Bruner et al., 1976; Brueckner et al., 1978). An empirical model, averaged over the entire extent of a sunspot, has been published by Cheng and Moe (1977) for the temperature range 4 10^4 to 2 10^5 K. Results for active regions in the corona have been obtained from high resolution soft X-ray observations (e. g. Landini et al., 1975; Davies et al., 1975).

For the present calculations we have adopted a model with constant conductive flux in the region of temperatures from 10^5 K up to coronal temperatures; the temperature gradient in this model is given by Eq. (9), which after integration gives:

$$T=\left[T_0^{7/2}+\frac{7}{2}\frac{F_c}{A}(z-z_0)\right]^{2/7}; \quad T_0<T<T_{cor}. \quad (13)$$

Here F_c is the conductive flux, $T_0=10^5$ K, T_{cor} is the coronal temperature, z_0 is the height at which $T=T_0$. Below T_0 we have used the temperature model of Cheng and Moe (1977) extrapolated down to 2 10^4 K; the atmosphere becomes optically thick above this level so we do not need to consider lower temperatures. The corona is assumed isothermal with $T_{cor}=2.6\ 10^6$ K. The exact value of T_{cor} is not important because the atmosphere becomes optically thin at these temperatures and its contribution to the brightness temperature is small.

Our density model is based on the assumption of hydrostatic equilibrium for the gas pressure. With the temperature given by

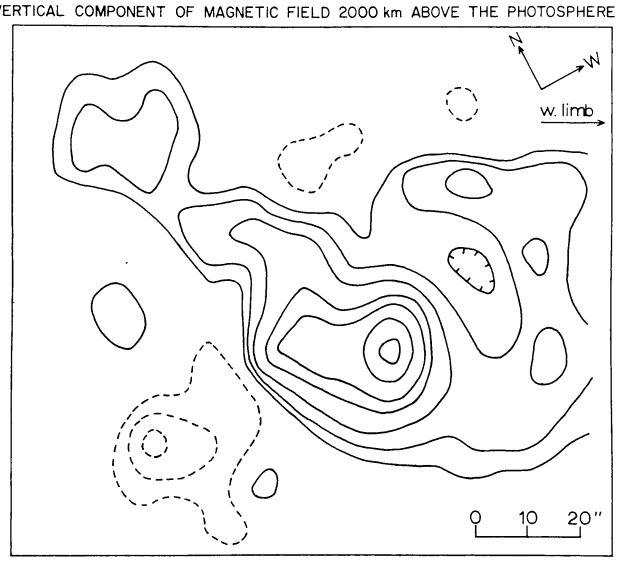

Fig. 5. Map of the vertical component of the magnetic field at 2000 km above the photosphere calculated under the current-free assumption. The region is the same as in Fig. 4; contour levels are ± 25, ± 50, ± 100, 200, 300, 500, and 700 G

Eq. (13) the pressure, P, is given by:

$$P = P_0 \exp\left(-8.9\ 10^{-11}\ [T^{5/2} - T_0^{5/2}]/F_c\right) \tag{14}$$

where P_0 is the pressure at height z_0 and F_c is in cgs units. We have assumed full ionization of He and He abundance of 0.1 relative to Hydrogen. The hydrostatic equilibrium model is not too different from the constant pressure model; indeed, for $F_c = 2.0\ 10^6$ the pressure drops only by a factor of 1.3 between 10^5 and $2\ 10^6$ K.

Our model leaves essentially three parameters to be determined from the observations: z_0, F_c, and P_0. Uncertainties arise from the assumption of constant F_c, the neglect of down flows of 10 to 100 km s^{-1} (Brueckner et al., 1978; Bruner et al., 1976) and the fact that we have completely ignored the presence of the strong magnetic field of the sunspot. If the T.R. is as extended as the extended as the observations of Foukal et al. (1974) indicate, the conductive flux will be lower than the radiative flux and it will not be constant (Foukal, 1976). Furthermore, the assumption of hydrostatic equilibrium may be invalid (Foukal, 1976; Bruner et al., 1976; Brueckner et al., 1978). On the other hand, the magnetic field will affect both the pressure structure and the coefficient A in Eq. (7). Therefore it should be emphasized here that we consider this model to be only a *working model,* its main advantages being its simplicity and the fact that it reproduces the temperature rise in the T.R.

b) Magnetic Field Model

Our observations give the longitudinal component of the photospheric magnetic field, while for our computations we need the vector magnetic field in the T.R. and the low corona. We have calculated the vector magnetic field by making the assumption that no currents flow above the photosphere. In this case the field is derived from a potential which is a solution of the Laplace equation. When the longitudinal component of the photospheric magnetic field, H_L, is used as a boundary condition the potential, ϕ, in plane geometry is given by (Semel, 1967):

$$\phi(x,y,z) = -\frac{1}{2\pi}\int_s\int \frac{\gamma r + z}{r(r+k)} H_{L^0}(x_0,y_0,z_0)\,dx_0 dy_0 \tag{15}$$

where

$$r^2 = (x-x_0)^2 + (y-y_0)^2 + z^2,$$

and

$$k = \alpha(x-x_0) + \beta(y-y_0) + \gamma z$$

α, β, and γ are the direction cosines of the line of sight in the coordinate system, x, y, z; the z axis is perpendicular to the solar surface and the x_0, y_0 plane is tangent to the solar surface. The components of the field are given by

$$\boldsymbol{H}(x,y,z) = -\nabla\phi(x,y,z). \tag{16}$$

A straightforward numerical calculation of the field from the above equations is very time consuming: if the observed field is an array of $N \times N$ points then for each point x, y, z and for each component we need N^2 operations, or $3N^4$ operations for the calculation of N^2 points at a given height. However, Eq. (15) is a convolution integral and can be calculated by using fast Fourier transform routines which greatly reduce the computation times.

The magnetic field has been computed at heights from 10^3 km to $8\ 10^3$ km in steps of 10^3 km and at $16\ 10^3$ and $32\ 10^3$ km; at intermediate heights the field was obtained from a cubic spline interpolation. Figure 4 shows a contour map of the longitudinal component of the photospheric magnetic field of the active region. As an example of our calculation we show in Fig. 5 the z component of the field at a height of $2\ 10^3$ km. Besides the smoothing effect of the convolution and the decrease of the field intensity, as compared with the photospheric field of Fig. 4, we may notice the disappearance of the negative polarity "island" in the west of the spot. This shows that the "island" is due to projection effects, as the field lines fan out near the edge of the spot.

V. Numerical Calculations

The integration of the transfer equation has been carried out, starting with the coronal contribution and proceeding downwards until the optical depth became greater than 10. The level of reflection at 6 cm occurs at $N = 3.1\ 10^{11}$ cm^{-3}, which is below the T.R.; in our region of interest the refractive index remains sufficiently close to unity, so that we can ignore the curvature of the rays.

The contribution of the corona has been calculated analytically as described in Sect. IIIa. The contribution of the T.R. was calculated by including the contribution of the $f-f$ process as well as the $g-r$ process from the second, third and fourth harmonics. Higher harmonics are transparent, while the field was too low to raise the fundamental in the T.R. For each point the heights of the resonance levels were calculated and the T.R. was split into $k+1$ layers, where k is the number of resonance levels that were contained in the T.R. The optical depths and the brightness temperatures of the resonance levels and of the $f-f$ layers were then calculated.

The $f-f$ absorption coefficient was taken from Zheleznyakov (1970) and the effect of He and metals was taken into account (Chambe and Lantos, 1971). The $g-r$ absorption coefficient was calculated by several authors (e.g. Gershman, 1960; Kakinuma and Swarup, 1962; Zheleznyakov, 1970; Kai, 1965). We used here the full expressions from Zheleznyakov (1970). For constant

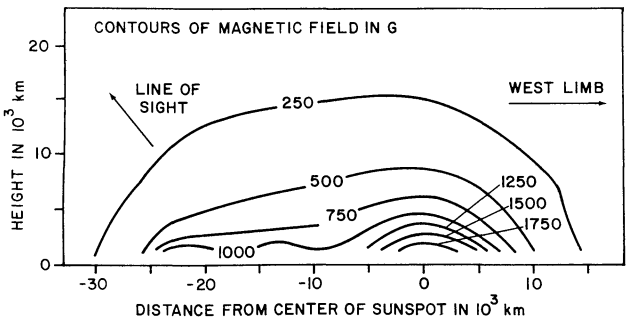

Fig. 6. Contours of equal magnetic field strength (labels in G) on a plane perpendicular to the solar photosphere through the center of the sunspot

temperature and density, the optical depth of a resonance level can be calculated analytically. In our model, however, there are regions where T and N vary by a significant amount within the layers; in such cases τ and T_b must be calculated numerically. We did the calculation numerically whenever the change of temperature over the FWHM of the layer was greater than 10%, or when the optical depth of the layer was greater than 5.

The calculations gave maps of brightness temperature of the two wave modes as a function of position. Since the propagation conditions are quasi-longitudinal in the sunspot associated region considered here, the total intensity and circular polarization are given by:

$$I=(T_{b,1}+T_{b,2})/2 \tag{17}$$

$$V=[(T_{b,1}-T_{b,2})/2]\,\frac{\cos\theta}{|\cos\theta|}. \tag{18}$$

The final step was the convolution of the maps with the interferometer beam which was carried out by means of fast Fourier transforms. The results are presented and discussed in the following section.

VI. Results and Discussion

In our choice of the best possible model, we have carefully considered some of the observed characteristic features of the source, namely the value of the peak brightness temperature, the double peaked circular polarization structure, the width of the source and the fact that both the total intensity and circular polarization decrease faster in the limbward side of the source (Fig. 1). All these features were reproduced in the model with $F_c=2\ 10^6$ erg cm^{-2} s^{-1}, $p_0=10^{15}$ cm^{-3} K and $z_0=2\ 10^8$ cm.

From the discussion in Sect. III it follows that $f-f$ emission alone cannot account for the observed value of the brightness temperature. On the other hand, the current-free magnetic field calculations did not give a sufficiently high magnetic field in the T.R. for effective $g-r$ emission. Therefore, we increased the value of the current-free magnetic field by a factor of 2.15. The origin of this discrepancy will be discussed later in this section; at this time we shall only discuss the results obtained with the adopted model.

a) Origin of Radiation and Comparison with Observations

Figures 6 and 7 show plots of some relevant quantities along a line through the brightest point of the source in the direction of the limb. Contour maps of the magnitude of the magnetic field on a plane perpendicular to the solar surface are shown in Fig. 6. Figure 7a gives the height of the $l=2$ and $l=3$ levels above the photosphere; Fig. 7b shows the angle θ between the direction of the magnetic field and the line of sight at the location of the second and third harmonics; Fig. 7c shows the contributions from the second and third harmonic levels to the brightness temperature of the extraordinary mode; and Fig. 7d shows the calculated brightness temperature of both modes before convolution with the interferometer beam.

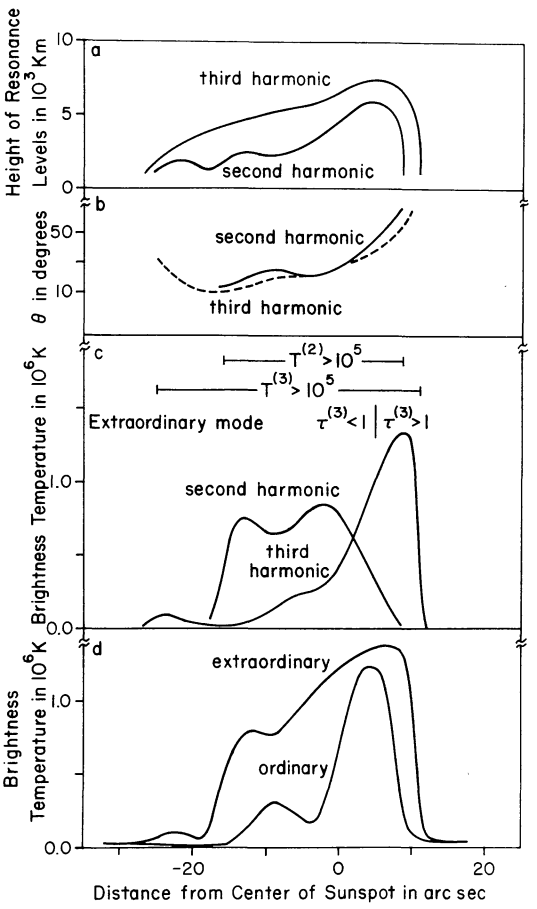

Fig. 7. Plots of a number of relevant quantities as a function of distance from the center of the sunspot. The magnetic field calculated from the current-free model has been multiplied by a factor of 2.15. **a** Height of the second and third harmonic levels. **b** Angle between the line of sight and the direction of the magnetic field at the location of the second and third harmonic levels. **c** Contribution of the second and third harmonic levels to the brightness temperature of the extraordinary mode. **d** Brightness temperature of the extraordinary and ordinary modes

The contribution of the $f-f$ process is small, about $3\ 10^4$ K, compared with the peak brightness temperatures of $1.4\ 10^6$ K for the extraordinary and $1.2\ 10^6$ K for the ordinary mode. For both modes the emission at the fourth harmonic is negligible, while for the ordinary mode the third harmonic emission is negligible too. As a result, the brightness temperature of the ordinary mode is determined by the second harmonic level, while both the second and third harmonics contribute to the brightness of the extraordinary mode; this is a direct consequence

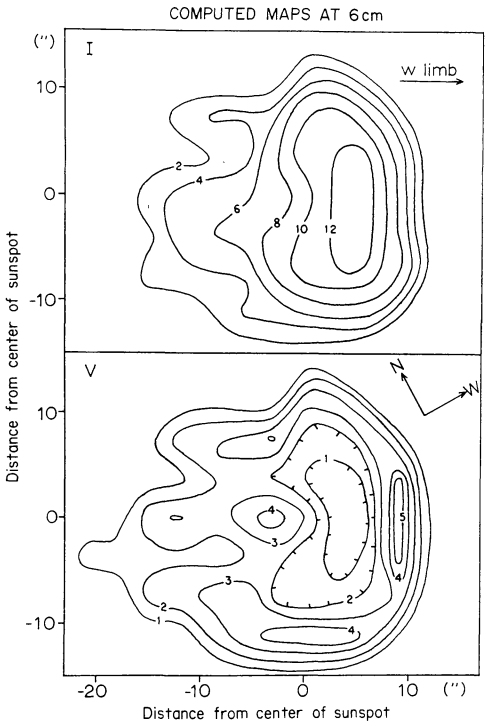

Fig. 8. Calculated I and V maps for the model described in the text. Contour labels are in units of 10^5 K; hatched contours show decreasing T_b. Notice the shell structure of the V map and the fast drop of T_b at the limbward side

of the higher opacity of the plasma to the extraordinary radiation. For significant emission a level must be located in a region of high T_e, (i.e. above the base of the T. R.) and it must be optically thick.

The brightness temperature of the ordinary radiation, $T_{b,2}$, is given approximately by the relation

$$T_{b,2}=T_e^{(2)}(1-\exp[-\tau_2^{(2)}]) \tag{19}$$

where $T_e^{(2)}$ is the electron temperature and $\tau_2^{(2)}$ the optical depth of second harmonic level. Since the temperature of a level varies in the same fashion as its height and the optical depth is determined primarily by the angle θ, the profile of $T_{b,2}$ (Fig. 7d) follows closely those of the height and θ (Figs. 7a and 7b). The maximum occurs at the location where the height of the second harmonic level is maximum.

The brightness temperature of the extraordinary mode, $T_{b,1}$, is given approximately by

$$T_{b,1}=T_e^{(2)}\exp(-\tau_1^{(3)})+T_e^{(3)}(1-\exp[-\tau_1^{(3)}]). \tag{20}$$

The terms on the right hand side are the contributions from the second and third harmonic levels respectively (second harmonic level is optically thick). These contributions are plotted in Fig. 7c as a function of position; on the same figure we have marked the region of $\tau_1^{(3)}>1$ and the regions over which T_e exceeds 10^5 K. The contribution of the second harmonic level follows the variation of height of the level (Fig. 7a) except on the west side of the region where the radiation is strongly absorbed by the 3rd harmonic level. The contribution of the third harmonic level follows the variations of both the height of the level and θ (Figs. 7a and 7b). The maximum occurs near the location of maximum height of the third harmonic level.

In both modes the brightness falls sharply on the limbward side, due to the fast decrease in height of the harmonic levels there (Fig. 7a). A comparison of Figs. 6 and 7a shows that this is purely a projection effect. Due to the same effect the source is displaced toward the limb with respect to the sunspot. We also note that the source is wider in the extraordinary mode; as a result the circular polarization map shows a shell structure, the degree of polarization being higher at the rim of the spot than at the center. This evident in Fig. 8 which shows I and V contour maps of the computed brightness temperature.

For comparison with observations we have presented in Fig. 9 contour maps of I and V after convolution with the WSRT beam. The maximum total intensity is $8.5\,10^5$ K, compared with the observed value of $8.6\,10^5$ K; the computed size (FWHM) of the radio source is $17''\times25''$, compared to the observed size of $17''\times28''$. At lower brightness temperatures, the observed size is larger than the calculated one since we have ignored the plage emission.

After convolution with the beam, the shell structure in the circular polarization map becomes a double-peaked structure; this happens because the beam is three times larger in the N-S direction than in the E-W direction. In agreement with observations the west peak is weaker; the computed values of polarization are higher than the observed ones by about 23% for the east peak and 6% for the west peak. The calculated size of the circularly polarized region at half intensity level is in good agreement with observations, but at lower intensity levels the observed source is wider because we have ignored the contribution of the plage.

b) Effect of Change of Model Parameters

Our computed maps are sensitive to the physical conditions in the temperature range 10^5 K to $1.3\,10^6$ K. In this region our model is determined by three parameters, F_c, p_0, and z_0, to which we added a fourth, the correction factor a for the intensity of the magnetic field. We shall now discuss how a change of these parameter affects the results, after ignoring the small contribution of the $f-f$ process.

The width of the source is about equal to the width of the region where the second harmonic level is located above the base of the T. R.; this is determined by a. To a lesser extent the width depends on the pressure: a 50% increase in p_0 increases the FWHM by 1″, the same as a 5% increase in a.

The brightness temperature, T_b, depends on the electron temperature, T_e of the harmonic levels and on the optical depth, τ. In terms of our chosen parameters, T_e depends on F_c, a, and z_0, while τ depends on all four parameters. At maximum T_b, τ is large, consequently $T_b=T_e$. Near the adopted values of the parameters, a 10% change in T_e can be produced by a 26% change in F_c, a 23% change in a or a 70% change in z_0. We have set z_0 to be equal to $2\,10^8$ cm, which is the value usually quoted in EUV results for the quiet Sun. Having determined a from the FWHM, we determined F_c from the maximum value of the observed T_b.

The pressure, p_0 affects the western polarization peak. Since both modes in this region originate in the third harmonic level, it is easy to see that in this case V has a maximum at a certain value of p_0, decreasing both for higher and lower pressure. Our adopted model is near this maximum; indeed, a change of p_0 by a factor of 5 in either direction makes the western V peak disappear.

In summary, F_c affects primarily the maximum value of T_b, a affects both T_b and size of the radio source and p_0 affects the circular polarization and size. Changes of F_c and a by $<20\%$ or

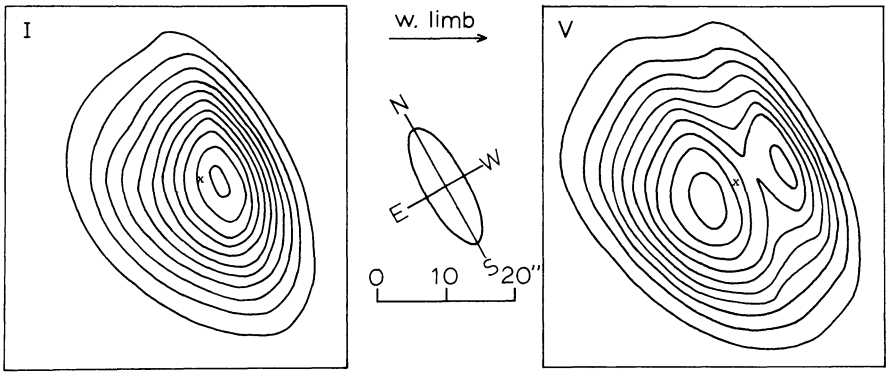

Fig. 9. Result of convolution of the maps in Fig. 8 with the WSRT beam pattern. Notice the double peaked structure in the V map (cf. Fig. 1). The contour levels are 7.5 10^4–8.25 10^5 K in steps of 7.5 10^4 K for the I map and 2.25 10^4 K to 2.25 10^5 K in steps of 2.25 10^4 K for the V map. The x's mark the center of the sunspot

Table 1. Empirical models of active regions from cm-λ, UV, and soft X-ray data

Author	Spectral region	F_c (erg cm^{-2} s^{-1})	p_0 (cm^{-3} K)	Remarks
Present model	6 cm	2 10^6	10^{15}	a, b, d, g
Chiuderi et al. (1971)	cm-λ	1.35 10^6	10^{16}	b, d, f
Felli et al. (1975)	1.8 cm, 3 cm	—	$>$ 5 10^{14} at $T_e=10^5$ K $>$ 3 10^{16} at $T_e=10^6$ K	f, h
Akhmedov et al. (1976)	cm-λ	$\sim$3.5 10^6 at $T_e=1.2\ 10^6$ K	3.8 10^{15} at $T_e=1.2\ 10^6$ K	a, g
Chiuderi-Drago et al. (1977)	2.8 cm, 21 cm	—	2.2 10^{16} at $T_e=2.2\ 10^6$ K	f, h
Noyes et al. (1970)	UV	3 10^6	3.6 10^{15}	b, d; Deduced values
Dupree et al. (1973)	UV	1.5 10^7	5.4 10^{15}	b, d
Jordan (1976)	UV	1.3 10^5 – 1.6 10^6	2 10^{15} – 2.9 10^{16}	b, d
Foukal (1976)	UV	4 10^4 at $T_e=6\ 10^5$ K	$<$ 7 10^{14} at $T_e<10^6$ K	a, c
Cheng and Moe (1977)	UV	2 10^5 at $T_e=2\ 10^5$ K	7.2 10^{14} at $T_e=2\ 10^5$ K	a, c, e
Parkinson (1973)	SXR	—	4 10^{15} – 6 10^{16} at $T_e=2\ 10^6$ – 6 10^6 K	
Landini et al. (1975)	SXR	—	5 10^{15} – 2.5 10^{16} at $T_e=2.2\ 10^6$ – 2.8 10^6 K	d; Maximum values for 8 regions
Davies et al. (1975)	SXR	—	10^{15} – 1.3 10^{16} at $T_e=2\ 10^6$ – 2.6 10^6 K	
Vorpahl (1978)	SXR	—	2.8 10^{15} – 1.5 10^{16} at $T_e=2.3\ 10^6$ – 3.7 10^6 K	Maximum values of one region over 3 d

[a] Model of region above sunspots
[b] Constant conductive flux model
[c] Constant total flux model
[d] Hydrostatic equilibrium assumed
[e] Constant pressure assumed
[f] Free-free process
[g] Gyroresonance and free-free processes
[h] Isothermal model

a change of p_0 by less than a factor of 5 would produce less than 10% change in the computed maps.

c) Origin of Correction Factor a

In this section, we consider whether the correction factor for the magnitude of the current-free magnetic field could come either from errors in the observations of the photospheric field or from the inadequacy of the current-free model. A saturation of the magnetograph could account for the correction factor; the Meudon magnetograph gives a maximum field strength of 1200 G, while the Rome Observatory gives 2000 G (Cassamasina and Croce, 1974) and Mt. Wilson (Solar Geophysical Data, 1974) gives 1600–2000 G for the same spot. However, as it was pointed out in Sect. II, the Meudon magnetograms are not affected by saturation; thus the instrumental origin of the correction factor is not very likely.

If the current-free assumption is not valid, the additional magnetic field strength that is required could be produced by currents of the order of 10^{12} A over a region of 10^9 cm in size. In terms of a force-free model this would imply a value of the parameter α of 7 10^{-10} cm^{-1}; the twist angle of the lines of force is $\tan^{-1}\{(\alpha L_H)^{-1}\}$, which gives a reasonable value of about 60° (Nakagawa and Raadu, 1972). Moreover, the required current

density of about $1\,\mu$ A cm^{-2} is close to the values obtained by Rayrole and Semel (1970) from observations of the transverse component of the magnetic field in a sunspot group.

Thus the correction factor is most likely due to non-potential magnetic fields. We should note, however that a force-free model would twist the magnetic lines of force and consequently change the angle θ. The angle θ, calculated from the present current-free model is responsible for the good agreement of the calculated shape of the source with the observations.

d) Comparison with Other Models

Although the present model is a simplified one (cf. Sect. IVa), it is instructive to compare our results with other cm-λ observations of active regions and with ultraviolet and soft X-ray models which give information about the T. R. and the low corona above active regions. Table 1 gives the conductive flux and electron pressure for several such models. The table is not intended to be complete, but rather to indicate the range of values of these quantities.

The only direct value of F_c available from cm-λ observations is from the eclipse data of a weak ($T_b \simeq 7\ 10^5$ K at 6 cm) region by Chiuderi et al. (1971); it is consistent with our value, within a factor of 2. Our estimate of F_c is also close to the one obtained from the temperature gradient given by Akhmedov et al. (1976); these authors have interpreted the cm-λ eclipse observations of the polarized portion of an active region in terms of the $g-r$ process. The values of p_0 derived from the $f-f$ process alone are about a factor of 10 larger than ours; this must be due to the fact that the $g-r$ process was neglected by Chiuderi et al.

The ultraviolet observations with moderate spatial resolution (Noyes et al., 1970) give "average" values of the quantities over active regions. Recent high resolution observations from Skylab (Foukal et al., 1974) indicate a slow rise of temperature (i.e. low F_0) and low densities in the T. R. above sunspots. The present results are intermediate between the average active region and individual spots.

Foukal (1976) gives a model with a loop of cool material extending upwards from the center of the spots; at a given height the temperature at the axis of the loop is less than 10^5 K, increasing to coronal values over a distance of 1–2 10^9 cm (14″ – 28″) from the axis. These cool loops show time variations and may not be visible in all spots at all times. If such a cool structure existed in the region of formation of the cm-λ radiation we would expect to observe a depression in the total intensity maps, provided that the size of the cool region was larger than the instrumental resolution. The scale of the structure given by Foukal (1976) is larger than our E-W resolution so that we should have been able to detect, if not a complete depression, at least a two peaked structure in the I maps. Such structures were not observed (cf. maps in paper I) with the possible exception of McMath region 12915 on May 9 and the west part of region 12906 on May 8.

A different model of active region EUV loops is given by Levine and Withbroe (1977); according to them the cool core of the loop is not more than about 10^7 cm (0″.2) in diameter, while several cool loop cores may be imbedded in single hot sheath. Such a model is not in conflict with the present cm-λ observations since such thin loops are well below our resolution.

The soft X-ray data give coronal densities ranging from values approximately equal to ours to more than a factor of ten larger. It is well known, however, that the soft X-ray emission comes primarily from coronal loops and not from the region directly above sunspots. A calculation of the $f-f$ optical depth of such loops at 6 cm from the X-ray data of Landini et al. (1975) gives values from 0.01 to 0.15, so that we should not expect much emission from these structures at 6 cm.

Some authors (e.g. Shmeleva and Syrovatskii, 1973), have pointed out that the parameters p_0, T_c, and F_c are not independent. The theoretical model of Shmeleva and Syrovatskii for $F_c = 2\ 10^6$ erg cm^{-2} s^{-1} requires $p_0 = 2.7\ 10^{15}$ cm^{-3} K at $T = 2.6\ 10^6$ K and $p_0 = 4\ 10^{15}$ cm^{-3} K at $T = 5\ 10^5$ K; both values are higher than the best fit value of $p_0 = 10^{15}$ cm^{-3} K of the present model, but still within the estimated uncertainty of a factor of five. If we adopted the model of Shmeleva and Syrovatskii with $p_0 = 3.2\ 10^{15}$ cm^{-3} K, we would obtain a smaller temperature for the region with $T < 10^6$ K and a higher temperature for the region with $T > 10^6$ K. This would give a steeper rise of the brightness temperature from the edge of the sunspot to the center but it would not affect the main features of the computed maps.

e) Measurement of Magnetic Fields Using cm-λ *Data*

In Paper I, we already discussed the possibility of using the cm-λ polarization maps as magnetograms of the T. R. and the corona. There is no doubt that cm-λ radiation contains information about the magnetic field; it should be pointed out, however, that contrary to the photospheric radiation, the cm-λ radiation is not formed in a thin layer of the atmosphere but in two layers of varying height from the solar surface. In any case, the presence of high brightness temperatures requires the presence of the $l=2$ or $l=3$ harmonic layers in the transition region or low corona and from this requirement an approximate value of the magnetic field can be deduced. Simultaneous measurements in soft X-ray and EUV that give T_e and N_e averaged over the line of sight can give precise information on which of the two levels $l=2$ and $l=3$ is optically thick, thereby giving a fairly precise estimate of the magnetic field strength in the T. R. and the corona. The polarity of the magnetic field can be determined from the sign of the circular polarization, provided that the radiation does not encounter a quasi-transverse magnetic field region (cf. Paper I). If high resolution observations were available at several wavelengths in the cm-λ region then we could construct three dimensional magnetic field structure, the third dimension being the height in the Sun's atmosphere. Such observations should be available with large synthesis instruments of the VLA type, where nearly simultaneous measurements can be made at two or three frequencies.

VII. Summary and Conclusions

The analysis of the high resolution observations of a sunspot-associated region at 6 cm, with simultaneous observations of the longitudinal component of the photospheric magnetic field has led us to the following conclusions:

1. The observed brightness temperature of the radiation at 6 cm cannot be accounted for in terms of the free-free process alone.

2. Model calculations assuming hydrostatic equilibrium and F_c = constant showed that the brightness structure of the source in total intensity and circular polarization V can be interpreted in terms of the gyroresonance process at the second and third harmonics of the gyrofrequency.

3. The magnetic field in the transition region is 900–600 G; this is about a factor of two higher than predicted by a current-free-model, but this can be accounted for by introducing currents above the photospheric level.

4. Assuming a plane-parallel, constant conductive flux and hydrostatic equilibrium model we obtained best agreement with the observations for $F_c = 2\ 10^6$ erg cm^{-2} s^{-1} and $N_e = 10^{10}$ cm^{-3} at $T_e = 10^5$ K. These values are between those of active regions and individual sunspots derived from EUV observations.

5. Our observations show no evidence for a cool region larger than about 6″ (4.4 10^8 cm) above the center of sunspots, contrary to the suggestion of Foukal (1976). An alternative model of several thin loops embedded in a common hot sheath (Levine and Withbroe, 1977) is not inconsistent with our observations. It would be interesting to calculate the cm-λ emission using more sophisticated models of the physical conditions, including the cool loops and the effects of material flows. However, the present resolution of the cm-λ observations and the lack of spectral coverage do not make such an effort worthwhile. Since the cool regions are not always visible in EUV observations it should be interesting to have simultaneous observations in both cm-λ and EUV.

6. High resolution cm-λ observations can give information about the magnetic fields and other physical conditions in the transition region. In particular, one should be able to obtain three dimensional magnetic field structures from high resolution observations at a number of frequencies in the cm-λ range.

Acknowledgements. The authors wish to thank Dr J. Rayrole of Meudon Observatory for his assistance with the magnetic field observations and Dr E. J. Schmahl for critical reading of the manuscript.

The research reported in this paper was in part done at the University of Maryland with support from NASA grant NGR 21-002-199 and NSF grant ATM 76-22415. One of the authors (C.E.A.) wishes to acknowledge support from the National Research Foundation of Greece. Computer time was provided by the University of Maryland Computer Science Center and by the University of Athens.

References

Akhmedov, Sh.B., Borovik, V.N., Ikhsanova, V.N., Nagnibeda, V.G., Peterova, N.G.: 1976, *Astron. Zh.* **53**, 812 (English Transl. in *Soviet Astron.* **20**, 460)

Alissandrakis, C.E.: 1977, Thesis, University of Maryland

Athay, R.G.: 1971, in *Physics of the Solar Corona,* p. 36, Macris, C. J., ed., D. Reidel, Dordrecht

Brueckner, G.E., Bartoe, J.-D., Van Hoosier, M.E.: 1978, Proc. of the OSO-8 Workshop, eds. Hansen and Schaffner

Bruner, Jr., E.C.: 1976, *Astrophys. J. Letters* **210**, L97

Cassamasina, F., Croce, V.: 1974, *Solar Phenomena,* No. 193, 5, Rome Observatory

Chambe, G., Lantos, P.: 1971, *Solar Phys.* **17**, 97

Cheng, C.C., Kjeldseth Moe, O.: 1977, *Solar Phys.* **52**, 327

Chiuderi, C., Chiuderi Drago, F., Noci, G.: 1971, *Solar Phys.* **17**, 369

Chiuderi Drago, F., Felli, M., Tofani, G.: 1977, *Astron. Astrophys.* **61**, 79

Davies, J.M., Gerassimenko, M., Krieger, A.S., Vaiana, G.S.: 1975, *Solar Phys.* **45**, 393

Dupree, A.K., Goldberg, L.: 1969, *Solar Phys.* **1**, 229

Dupree, A.K., Huber, M.C.E., Noyes, R.W., Parkinson, W.H., Reeves, E.M., Withbroe, G.L.: 1973, *Astrophys. J.* **182**, 321

Felli, M., Poletto, G., Tofani, G.: 1977, *Solar Phys.* **51**, 65

Felli, M., Tofani, G., Fürst, E., Hirth, W.: 1975, *Solar Phys.* **42**, 377

Foukal, P.V.: 1975, *Solar Phys.* **43**, 327

Foukal, P.V.: 1976, *Astrophys. J.* **210**, 575

Foukal, P.V., Huber, M.C.E., Noyes, R.W., Reeves, F., Schmahl, E.J., Timothy, J.G., Vernazza, J.E., Withbroe, G.L.: 1974, *Astrophys. J.* **193**, L143

Gershman, B.N.: 1960, *JETP,* **38**, 912 (English Transl. in *Soviet Phys. – JETP* **11**, 657)

Jordan, C.: 1976, *Phil. Trans. Roy. Soc. London* **281**, 391

Kakinuma, T., Swarup, G.: 1962, *Astrophys. J.* **136**, 975

Kundu, M.R.: 1959, *Ann. Astrophys.* **22**, 1

Kundu, M.R.: 1965, Solar Radio Astronomy, New York, Interscience

Kundu, M.R., Alissandrakis, C.E.: 1975, *Nature* **257**, 5526

Kundu, M.R., Alissandrakis, C.E., Bregman, J.D., Hin, A.C.: 1977, *Astrophys. J.* **213**. 278 (Paper I)

Landini, M., Monsignori Fossi, B.C., Kreiger, A., Vaiana, G.S.: 1975, *Solar Phys.* **44**, 69

Lantos, P.: 1968, *Ann. Astrophys.* **31**, 105

Levine, R.H., Withbroe, G.L.: 1977, *Solar Phys.* **51**, 88

Nakagawa, J., Raadu, M.A.: 1972, *Solar Phys.* **25**, 127

Noyes, R.W., Withbroe, G.L., Kirshner, R.P.: 1970, *Solar Phys.* **11**, 388

Parkinson, J.H.: 1973, *Solar Phys.* **28**, 487

Rayrole, J.: 1967, *Ann. Astrophys.* **30**, 257

Rayrole, J., Semel, M.: 1970, *Astron. Astrophys.* **6**, 288

Semel, M.: 1967, *Ann. Astrophys.* **30**, 513

Shmeleva, O.P., Syrovatskii, S.I.: 1973, *Solar Phys.* **33**, 341

Solar Geophysical Data: 1974, No. 359, Part I, U.S., Dept. of Commerce, p. 86

Vorpahl, J.A.: 1978, *Solar Phys.* **57**, 297

Withbroe, G.L.: 1970, *Solar Phys.* **11**, 42

Zheleznyakov, V.V.: 1962, *Astron. Zh.* **39**, 5 (English transl. in *Soviet Astron.* **6**, 3)

Zheleznyakov, V.V.: 1970, Radio Emission of the Sun and Planets, Oxford, Pergamon Press

Zlotnik, E.Ya.: 1968a, *Astron. Zh.* **45**, 310 (English Transl. in *Soviet Astron.* **12**, 245)

Zlotnik, E.Ya.: 1968b, *Astron. Zh.* **45**, 585 (English Transl. in *Soviet Astron.* **12**, 464)